Gong JM, Yang H, Lin SH, Li R, Zivkovic V.

Spatial filtering velocimetry for surface velocity measurement of granular flow.

Powder Technology 2018, 324, 76-84.

Spatial filtering velocimetry for surface velocity measurement of granular flow

J. M. Gong[a], H. Yang[ab*], S. H. Lin[a], R. Li[a], V. Zivkovic[c]

a. School of Optical-Electrical and Computer Engineering, University of Shanghai for Science and Technology, Shanghai 200093, China

b. Shanghai Key Lab of Modern Optical System, University of Shanghai for Science and Technology, Shanghai 200093, China

c. School of Chemical Engineering and Advanced Materials, Newcastle University, NE1 7RU, United Kingdom

(Received)

Corresponding author: yanghui@usst.edu.cn

Abstract: In this study, we develop the spatial filtering velocimetry (SFV) technique to measure the velocity distribution of small spherical and irregular particle flows using a linear CCD camera. In addition, energy barycentre correction algorithm is used to enhance the measurement accuracy. A constantly running conveyor belt is used to test the accuracy of this SFV system. Furthermore, the velocity distributions of the spherical and irregular particle flows in a rotating drum are measured to demonstrate the usability of this method in a granular system. We further discuss the effect of the key system parameters on the results of the measurement, and the optimal thresholds of the parameters are given in this paper.

I. INTRODUCTION

Granular flows are ubiquitous in nature (rock and snow avalanches, movement of sand dunes) and in industrial processes (transport of food grains, ores, pharmaceutical powders). However, the mechanics of these material flows are not well understood. Knowledge of particle or particle cluster velocities in granular systems is essential to characterize the flow conditions and dynamics [1]. Particle image velocimetry (PIV) and particle tracking velocimetry (PTV) are two of the most widely used technologies for the measurement of the velocity and its distribution of granular flows [2-11]. However, PTV technique is suitable only to the conditions that each particle can be distinguished clearly which puts huge demand on image resolution and more importantly computing power for particle tracing which limits practical application to the larger particles. In the case of PIV, there is no demand to distinguish each particle but hands-on guidance is to have at least 3-4 pixel per particle size in each direction [8, 11]. However, large signal-to-noise of recorded images is desirable requiring for example uniform illumination, which is difficult to obtain due to complex interaction of imaging and lighting system with the observed particles, and accompanying scene [8, 11]. The further demand for PIV is to have at least 10 particles with recommendation to have 100 particle in interrogation window to avoid unreliable analysis and spurious results [8, 11]. Therefore, the PIV provides average velocity of particles in an interrogation window meaning the lower spatial resolution in the context of dense granular flow. This averaging also put limits on the technique applicability such as for example the case of granular temperature determination as a second order statistics measurement [10]. Other imaging methods like streak velocimetry [12, 13] and Voronoï imaging [14] are also used for granular flow studies which are more similar to PTV than to PIV, thus having the same issue of clear individual particle imaging. Laser Doppler velocimetry is another widely used method for the measurement of solid or fluid velocities with tracer particles [6]. However, it is also not suitable for the dense granular flow due to high concentration of the particles and resulting strong light scattering with occasional application for dense granular flow [6]. Recently, we used another laser-based technique of speckle visibility spectroscopy for study of surface granular flow due to very good spatial and temporal resolution [15, 16]. The limitation is that only granular temperature of particles can be measured, but not the actual particle velocities.

On the other hand, the spatial filtering velocimetry (SFV) technique has not received much attention from researchers since its inception, though the method was proposed by Ator [17] in 1963. In comparison with the Doppler and PTV as single tracer measurement methods, the method using a spatial filter is inferior with regard to spatial resolution like PIV as both are based on analysis of interrogation region in the images. However, this method has several useful features such as simplicity, optical system stability, and applications to nearly every reflective object. In addition, the technique can resolve the problem of low signal-to-noise ratio (SNR) of the signal, e.g. because of the non-uniform illumination, as well as from other factors [18]. It has been successfully applied to the velocity measurement of solid surfaces [19, 20], fluids [21-25], two-phase flows [26], and image motion, as well as other applications [27, 28]. Asakura used SFV to measure the liquid flow velocity in a 0.13–3.3-mm capillary glass tube based on an optical system with a microscope [23]. Aizu et al. improved the SFV and built a differential spatial filtering velocimeter based on the transmission grating; this structure could eliminate the low-frequency components of the signal, and they proved the validity of the method in the aspect of blood flow velocity measurement [18, 23]. Bergeler et al. used a CMOS array camera to simulate the function of a spatial filter device, and they achieved the measurement of the two-dimensional velocity component [22]. By making use of the experimental system, they measured the blood flow velocity distribution in a capillary tube. Wang et al. used a CCD-array simulated spatial filter and applied the SFV to the average velocity measurement of nanofluids, and they achieved a relative error of less than 6.5% [25]. Xu et al. used an electrostatic sensor array as a spatial filter to obtain the velocity of gas–solid two-phase flow particles in a pipeline. To a certain extent, they realized the measurement of the local average velocity of the particles [29, 30]. However, this may be due to the complex nature of the particles, non-constant particle velocity, and set-up difficulty of the measurement system; there are few reports on the particle velocity distribution in a fluidized bed.

In this study, we develop the SFV technique to measure the velocity of granular materials of irregular sand particles. The energy barycentre correction algorithm is used to enhance the frequency accuracy. A constantly running conveyor belt is used to test the accuracy of the SFV system. Then, the velocity distributions of the small spherical and irregular particle flows in a rotating drum are measured using the SFV method. Finally, we discuss the effect of the system parameters on the measuring result, and the optimal thresholds of the parameters are given in this paper.

II. PRINCIPLES OF SPATIAL FILTERING VELOCIMETRY (SFV)

A. Basic principle of SFV

Figure 1 shows a schematic of a traditional SFV comprising an objective lens, transmission grating, focusing lens, photoelectric sensor, and light source. The light source irradiates a moving surface with velocity v. Part of the reflected light from the moving surface is collected by the objective lens. The surface is imaged onto a spatial filter, which has a spatially periodic transmittance in the moving direction of the surface. The total light intensity collected by the focusing lens is temporally periodic because of the motion of the moving surface. Then, the temporally periodic light intensity is fed into the photodetector. As a result, the output signal of the photodetector contains a centre frequency f relative to the velocity v of the moving surface. Then, the relationship between the moving surface velocity v and centre frequency f can be determined as follows [18]:

$$v = \frac{pf}{M} \tag{1}$$

where p is the spatial period of the spatial filter and M is the magnification of the optical system.

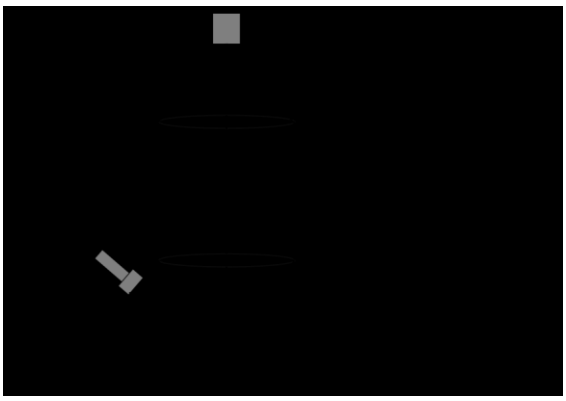

Fig.1 Schematic of spatial filtering velocimeter

Because of the characteristics of complex structure, processing difficulty, and spatial period instability, the traditional SFV system with a transmission grating and photoelectric sensor structure has been replaced gradually by linear or CCD/CMOS array cameras [20-23]. The utilization of the image sensor greatly simplifies the system structure and improves the characteristics of flexibility and stability.

B. Principle of SFV based on linear CCD

In this approach, a linear CCD camera is used as both a spatial filter and optoelectronic transform device. Figure 2 shows a schematic of the spatial filter simulated by the linear CCD. The spatial filter has a size of X pixels in the x-direction and Y (for the linear CCD, Y = 1) pixels in the y-direction, and all the pixels of the spatial filter can be divided into $2n$ groups whose size is b pixels. As shown in Fig. 2, the combination of every other pixel group, in other words, odd groups (grey space) and even groups (white space), is equivalent to the spatial filters S_w and S_g on the structure, respectively. The spatial period, p, of the spatial filters, S_w and S_g, is equal to $2b$ pixels. For S_w, the white regions allow light to pass through, while the grey regions block the light. For S_g, the opposite is true.

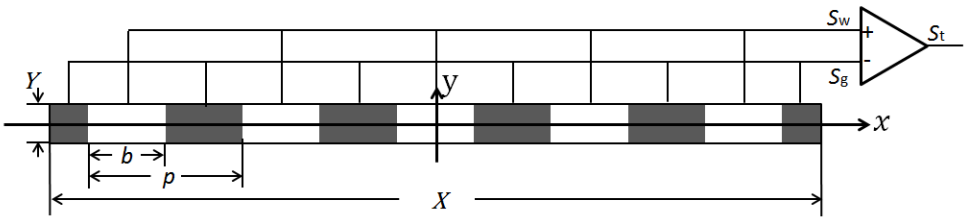

Fig.2 Schematic of spatial filter simulated by linear CCD

In the process of data processing, the output of the spatial filter:

$$S_w = \sum_{i=1}^{n} w_i \quad (2)$$

$$S_g = \sum_{i=1}^{n} g_i \quad (3)$$

The spatial filters S_w and S_g combine into a differential spatial filter and the output of the differential spatial filter S_t is equal to $S_w - S_g$. The differential spatial filter can greatly eliminate the residual signal of the base component and the problem of low SNR of the output signal from non-uniform illumination , as well as from other factors [18].

C. Characteristics of spatial filter based on linear CCD

Let the light intensity transmittance function of the spatial filter based on the linear CCD and the light intensity distribution of the moving surface image at the plane of the CCD be $t(x, y)$ and $h(x, y)$, respectively. The output

signal $g(x,y)$ obtained from the CCD image sensor is given by the convolution integral of $t(x,y)$ and $h(x,y)$. In the spatial frequency domain, $T(\mu,\nu)$ is the Fourier transform of $t(x,y)$, $H_p(\mu,\nu)$ is the power spectral density function of $h(x,y)$, and $G_p(\mu,\nu)$ is the spatial power spectral density function of $g(x,y)$. $G_p(\mu,\nu)$ can be represented as [22]:

$$G_p(\mu,\nu)= H_p(\mu,\nu)|T(\mu,\nu)|^2 \tag{4}$$

where μ and ν denote the spatial frequencies in the x- and y-directions, respectively.

As shown in Eq. 4, the frequency spectrum $|T(\mu,\nu)|^2$ acts as a spatial filtering function on the input function $H_p(\mu,\nu)$. Therefore, the characteristics of the frequency spectrum $G_p(\mu,\nu)$ can be investigated from the frequency spectrum $|T(\mu,\nu)|^2$ of the spatial filter. The frequency spectrum $|T(\mu,\nu)|^2$ can be represented as [20]:

$$|T(\mu,\nu)|^2 = \frac{X^2Y^2}{4}|T_Y(\nu)|^2\left|\sum_{n=1}^{2n}(-1)^{n-1}\frac{4}{(2n-1)\pi}[T_{Xn}^{-}(\mu)+T_{Xn}^{+}(\mu)]\right|^2 \tag{5}$$

where

$$T_Y(\nu) = \sin c(\nu Y) \tag{6}$$

$$T_{Xn}^{-}(\mu) = \sin c(\mu X - \frac{2n-1}{p}X) \tag{7}$$

$$T_{Xn}^{+}(\mu) = \sin c(\mu X + \frac{2n-1}{p}X) \tag{8}$$

From Eqs. (5)–(8), it can be seen that the key parameters affecting the spatial filtering characteristics are the size of the spatial filter in the x- and y-directions, X and Y, and the number of slits, *n*, which will be discussed in section 4.

D. Spatial filtering data processing

The frequency spectrum of the differential signal, obtained by the Fast Fourier Transform (FFT) algorithm, can be represented as:

$$S_k = \left|\sum_{t=0}^{N-1} S_t \exp(-j2\pi kt/N)\right| \tag{9}$$

where S_t is the time-domain signal and N is the FFT point k = –N, –N+1, …, N–1.

For the moving object with uniform velocity (*i.e.* conveyor belt in this experiment), the centre frequency f can be obtained from the peak of the spectrum, as shown in Fig. 3 (a). For the particle system, however, the spectrum is expanded and noisy because of the velocity disorder of the particles in the measurement area, as shown in Fig. 3 (b). A correction to the FFT spectrum is required before the centre frequency is extracted from the peak of the spectrum [25, 31].

There are several frequency spectrum correction algorithms, such as the energy barycentre correction, ratio correction, phase difference correction and ZOOM FFT algorithm [32-38]. The energy barycentre correction method does not depend on the window function, and can correct the multi-stage average power spectrum directly, the algorithm is simple and easy to implement, the correction accuracy is related to the number of points which participate in the correction, the more points, the higher correction accuracy [32, 33]. The ratio correction can correct frequency, amplitude and phase and the precision of refining effect is high, and not applicable in too dense frequency analysis [36]. The phase difference correction algorithm is more versatile with high correction accuracy and simple calculation method. It is suitable for the correction of the discrete frequency components with frequency

spacing greater than five frequency resolutions. If the frequency components are too close, there would be the side lobe interference and even main lobe interference, which can affect the calibration accuracy and even cannot be corrected [35, 37]. The ZOOM FFT algorithm is both accurate and easy to use, accurate results would be expected in most cases with the method being superior to the simple estimation procedures commonly used. This method can increase the resolution of the amplitude spectrum, but it cannot be certainly effective in diminishing the phase distortion [34].

The energy barycentre correction is a suitable method in SFV because it has a simple algorithm, a small amount of computation, and a small error. In the process of spectrum correction, the energy barycentre correction algorithm is proposed to obtain a more accurate frequency value. The energy barycentre correction is realized by the following steps. First, use the average correction method to obtain the trend of the spectrum. Figure 3(b) shows an example result of the average method for frequency spectrum correction. The black curve represents the signal spectrum before correction and the red curve represents that after correction. Second, use the energy barycentre correction [38]technique to determine the peak frequency bin in the frequency spectrum after average correction. Then, find the largest part of the peak frequency bin. Finally, calculate the centroid of the frequency bins and set the position of the centroid as the corrected frequency bin, which is regarded as the centre frequency of the time-domain signal.

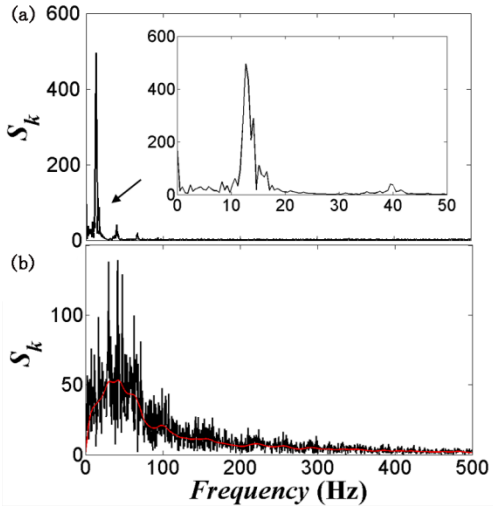

Fig.3 Example of frequency spectrum of the signal from (a) conveyor belt and (b) particle system.

Inset: Magnification of (a) in the frequency range from 0 to 50 Hz

E. Velocity distribution measurement

Figure 4 shows a schematic of the velocity distribution measurement by multipoint measurement. The average velocity of the sub-area on the moving surface, centred at P_i, is measured by a sub-spatial filter SP_i, centred at P_i' comprised of X pixels, in the linear CCD camera. In addition, the velocity distributions of the moving surface along the x-direction are measured by the sub-spatial filters along the linear CCD. In addition, the spatial period, p, and the number of slits, n, of the sub-spatial filter SP_i have the relation $X = n * p$.

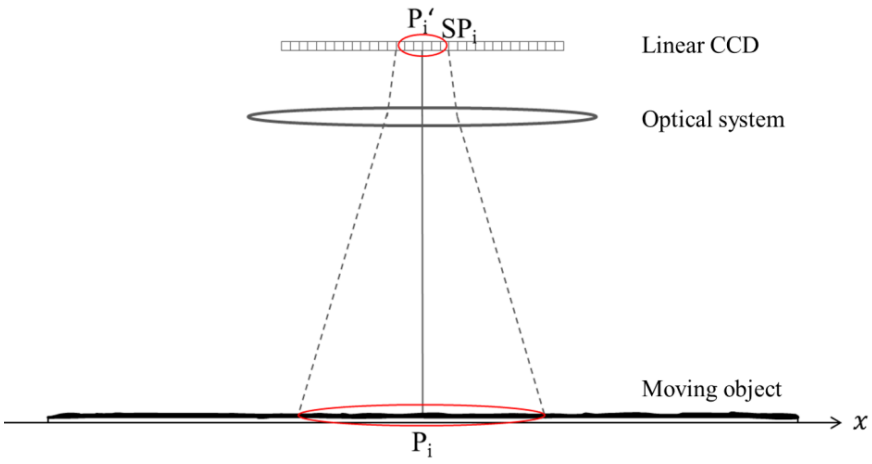

Fig.4 Schematic of velocity distribution measurement by SFV

III. EXPERIMENT AND RESULTS

A. Experimental setup

Figure 5 illustrates the measurement experimental setup of the SFV system with the specifications listed in Table 1. The system comprises a cylindrical drum, which is made of clear Plexiglas to allow optical access and has an inner diameter, D, and length, L, of 150 and 200 mm, respectively. The drum is placed on a pair of rollers, which are connected through a conveyor belt driven by a high precision and high-stability DC motor. The conveyor belt is also used as the standard speed for the test. The linear CCD camera and lens are fixed to the bracket, the shooting angle is adjusted to ensure the camera is perpendicular to the object to be tested, and the x-direction of the linear CCD sensors is parallel to the direction of the moving object.

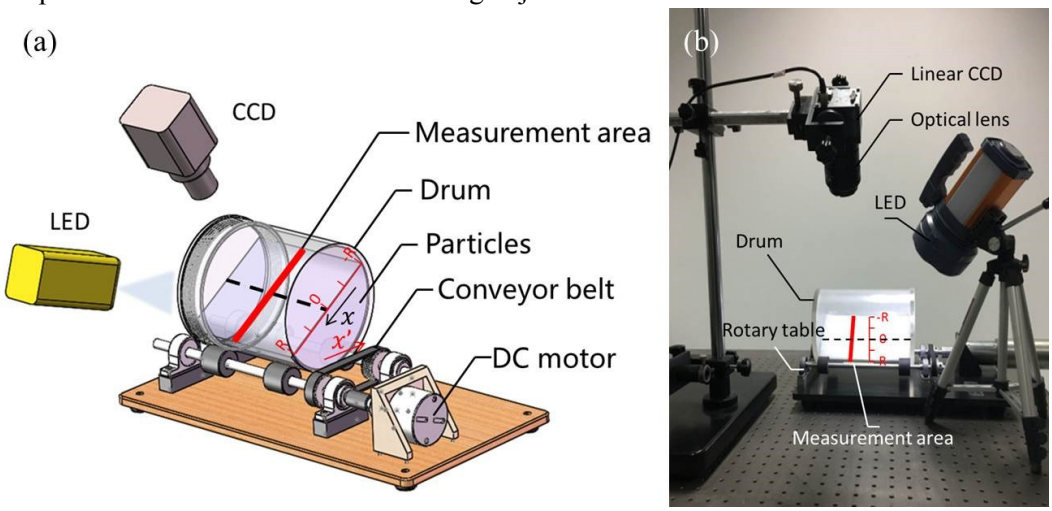

Fig.5 Particle velocity measurement system based on linear CCD SFV.

(a) Structural diagram and (b) diagram of experimental device.

The CCD camera is set to capture images of the moving objects with a sampling frequency f_s = 1000 Hz, and an Ethernet interface is used to transfer the image onto a computer.

Table.1 System specifications

Imaging system	
Focal length	35 mm
Magnification	0.915
CCD camera	
Number of pixels	1024
Pixel size	14*14 μm
Max frame frequency	56 kHz
Sampling frequency f_s	1000 Hz
Precision turntable	
Input voltage of DC motor	0–40 V
Reducer gear ratio	72:1
Roller diameter	3.6 cm
Drum & Particles	
Drum diameter	15 cm
Particle material	Spherical/irregular glass sands
Particle size	1–1.5 mm
Filling level	40%
FFT	
Number of data	1024

B. Granular materials

The granular materials used in this study are sieved glass beads and sand with a density of 1710 kg/m^3 between sieves of 1.0 and 1.5 mm, giving a median particle diameter of 1.25 mm, as shown in Fig. 6. All the granular materials used in this study were dry, cohesionless glass particulate materials. The filling level of the cylindrical drum was 50% of its volume.

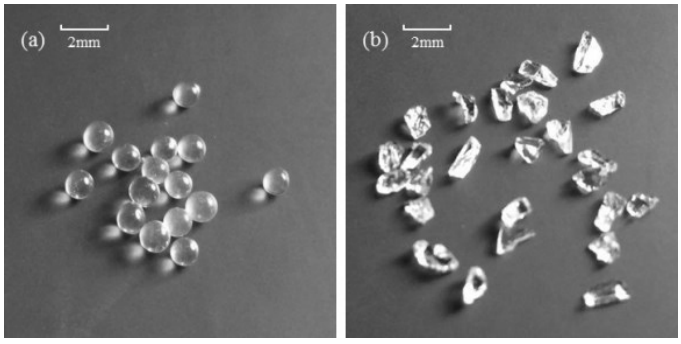

Fig.6 Example photo of particles with 2-mm scale bar. (a) Glass beads and (b) glass sand.

C. Results of test by conveyor belt

Figure 7 displays the original image collected by the linear CCD camera from the conveyor belt with the sampling frequency fs = 1000 Hz. As the conveyor belt velocity is constant, this leads to the appearance of inclined stripes in the original image.

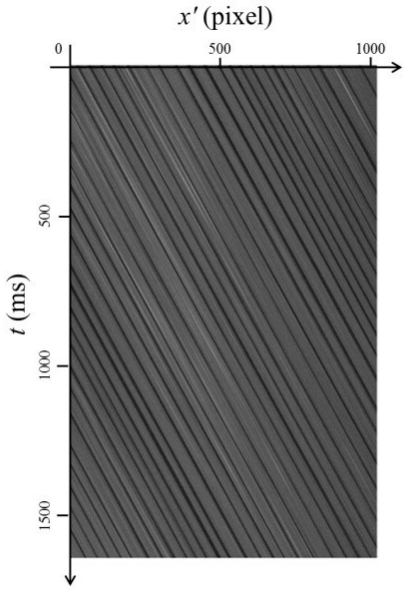

Fig.7 Original image collected by the linear CCD

Figure 8 presents the results of the average measurement velocities with the increase in conveyor belt speed with parameters of spatial period p = 16 pixels and number of slits n = 20. Table 2 presents the statistical results of the measurement indicating that the relative error is within 3%. It proves the feasibility of the spatial filtering velocity measuring system.

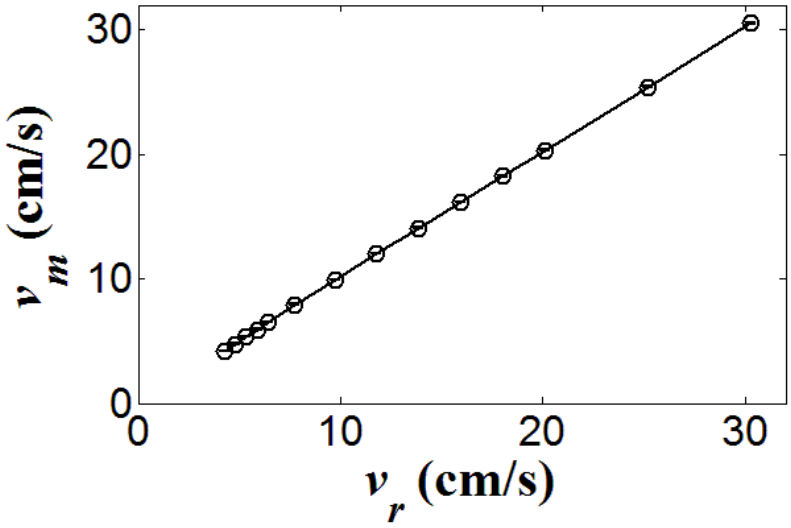

Fig.8 Average measurement results of 10 measurements vs. conveyor belt speed. The solid line represents the linear fit to the data. The error bars represent the standard deviation of the results and are so small that they are within the circles.

Table.2 Measurement results of 10 measurements with conveyor belt speed

No.	Speed of conveyor belt v_r（cm/s）	Average of measuring result v_m（cm/s）	Standard deviation	Relative error (%)
1	4.27	4.18	0.02	2.11
2	4.81	4.75	0.03	1.25
3	5.34	5.36	0.03	0.37
4	5.87	5.93	0.02	1.02
5	6.41	6.50	0.03	1.40
6	7.73	7.92	0.030	2.43
7	9.72	9.89	0.030	1.70
8	11.76	12.05	0.021	2.46
9	13.83	14.08	0.028	1.81
10	15.93	16.17	0.032	1.56
11	18.02	18.26	0.034	1.33
12	20.13	20.33	0.021	0.99
13	25.16	25.38	0.051	0.84
14	30.29	30.55	0.048	0.86

Figure 9 and Table 3 present the measurement results from different positions of the conveyor belt using the velocity distribution method described in section 2.5. It can be observed that the aberration of the measured velocities from the moving velocities of the conveyor belt is within 0.01 cm/s and the relative error is within 0.3%. This implies that in the field of view of the SFV based on the linear CCD, each point measurement result remains consistent.

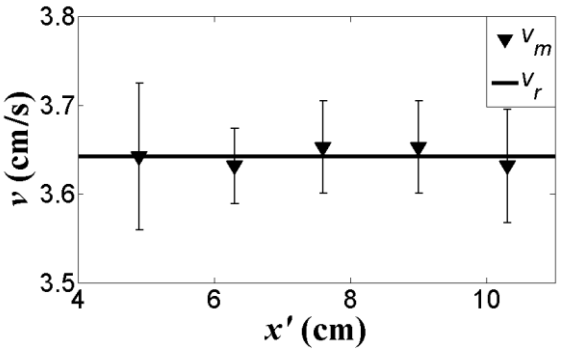

Fig.9 Average measurement velocities of 10 measurements at different positions of conveyor belt. The error bars represent the standard deviations of the results and the solid line indicates the real velocity (i.e. 3.64 cm/s) of the conveyor belt.

Table.3 Average measurement results of 10 measurements at different positions of the conveyor belt with speed of 3.64 cm/s.

Measurement point x' (cm)	Measuring result v_m（cm/s）	Standard deviation	Relative error (%)
4.9	3.64	0.08	0
6.3	3.63	0.04	0.27
7.6	3.65	0.05	0.27
9.0	3.65	0.05	0.27
10.3	3.63	0.06	0.27

D. Spherical particle velocity measurement experiment

Figure 10(a) displays the original image collected by the linear CCD camera from the spherical particle velocity measurement experiment, as shown in Fig. 5, with the sampling frequency f_s = 1000 Hz. As the particles are under the rolling regime in the rotating drum, this leads to the appearance of intermittent stripes in the original image.

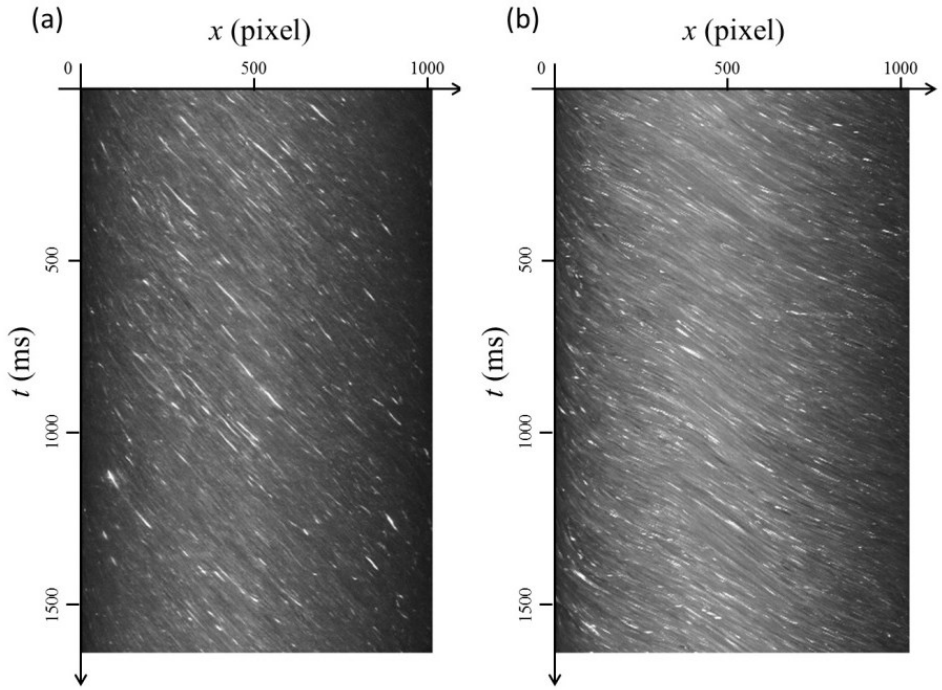

Fig.10 Original image collected by linear CCD in the particle velocity measurement experiment with (a) 1.25 mm spherical particles, (b) 1.25 mm irregular particles.

Figure 11 indicates that the average particle velocity increases linearly with the rotating velocities of the drum at the measurement point of x = 4 cm with the parameter spatial period p = 24 pixels and the number of slits n = 10, which agrees with the theoretical analysis of Jain et al. [39].

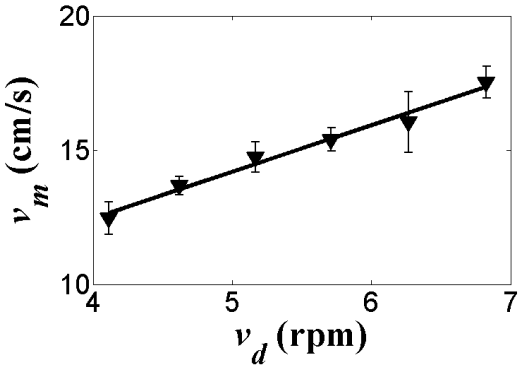

Fig.11 Average measurement results of 10 measurements vs. the rotating velocities of the drum. The triangle points represent the average of 10 measurements, while the error bars at each data point represent the standard deviation of 10 measurements. The solid line indicates the moving velocities of the particles with the increase in rotating velocity of the drum.

Figure 12 shows the particle velocity distribution in the *x*-direction of the drum at a rotating velocity of 5.2 rpm. It is clear that from the top to bottom of the velocity distribution, it is approximately symmetrical about the middle position and skewed. The experimental results also agree with the experimental results of the PEPT method by Ding et al. [40]. In addition, their research demonstrates that at low rotational speeds, the bed surface velocity profile is approximately symmetrical with respect to the mid-chord position, and with the increase in rotating velocities, a skewed surface velocity distribution is observed.

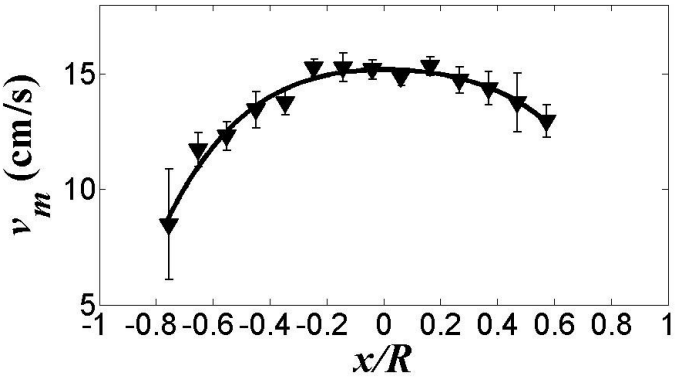

Fig.12 Spherical particle velocity distribution in the radial direction of the drum at a rotating velocity of 5.2 rpm. The error bars at each data point represent the standard deviation of 10 measurements. The solid line which is obtained by curve fitting indicates the spherical particle velocity distribution in the radial direction of the drum.

E. Irregular particle velocity measurement experiment

Figure 10(b) displays the original image collected by the linear CCD camera from the 1.25 mm irregular particle velocity measurement experiment, as shown in Fig. 5, with the sampling frequency *fs* = 1000 Hz. As the particles are under the rolling regime in the rotating drum and the velocity changes during the movement, this leads to the appearance of intermittent curves in the original image.

The velocity and its distribution of irregular particles under the rolling regime in the rotating drum are also measured by the SFV system depicted in Fig. 5, with parameters of spatial period *p* = 24 pixels and number of slits *n* = 10. Figure 13 indicates that the average particle velocity increases linearly with the rotating velocities of the drum at the measurement point of *x* = 4 cm, which is similar to the spherical particles.

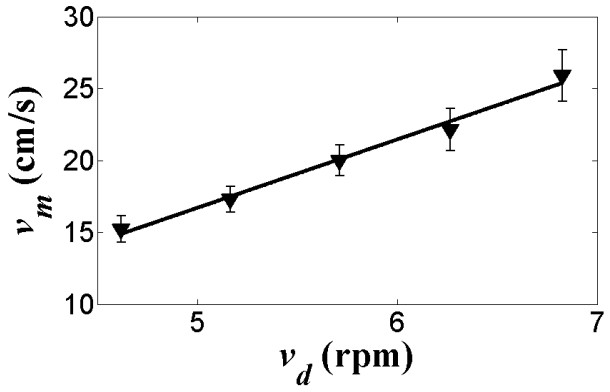

Fig.13 Average measurement results of 10 measurements vs. the rotating velocities of the drum with 1.25 mm irregular sands. The triangle points represent the average of 10 measurements, while the error bars at each data point represent the standard deviation of 10 measurements. The solid line represents the linear fit to the data.

Figure 14 shows the particle velocity distribution in the *x*-direction of the drum at a rotating velocity of 5.2 rpm, which indicates that the particle velocity initially increases and then gradually decreases after reaching the first peak at the upper part of the surface, while at the lower part of the surface, the particle velocity initially increases and then gradually decreases after reaching the second larger peak value. These results are similar to our previous observation [16] that the particle velocity is lower at the upper part than at the lower part of the surface because of a small mound forming at the approximate centre of the surface. The error bars of the first and last measurement points are larger than the others because of the influence of the cylinder walls. Comparing this result with Fig. 12, we can further find that the velocity of irregular particle flow is higher than that of the spherical particle flow at the same drum speed. This is also in line with the previous reports that the angle of repose of irregular particles is higher than that of the spherical particles [40, 41].

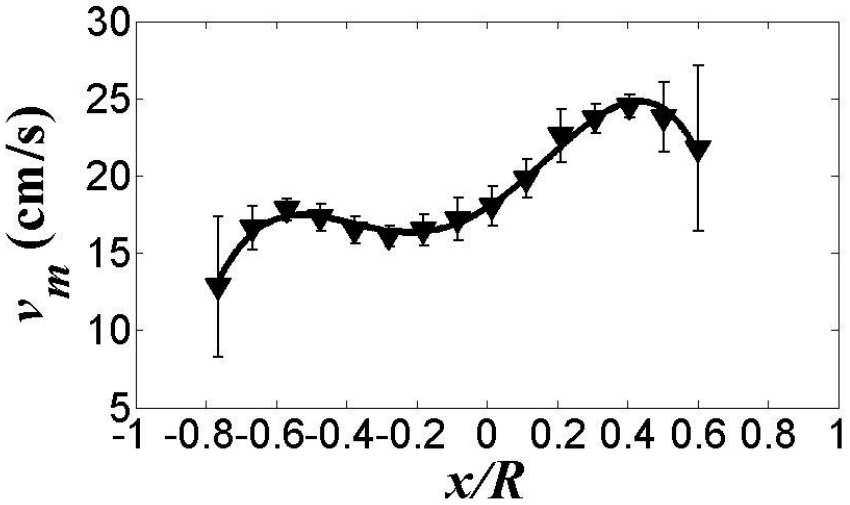

Fig.14 Particle velocity distribution in the radial direction of the drum with 1.25 mm irregular sands at a fixed rotating velocity of 5.2 rpm. The error bars at each data point represent the standard deviation of 10 measurements.

Figure 15 shows the particle velocity distribution in the *x*-direction of the drum at different rotating velocity from 5.2 rpm to 6.3 rpm, which indicates that with the increase of the rotating velocity of the drum, the particle velocity increased in each position of the drum. It indicated that the kinetic energy of irregular particle flow increase with the increase of rotating velocity.

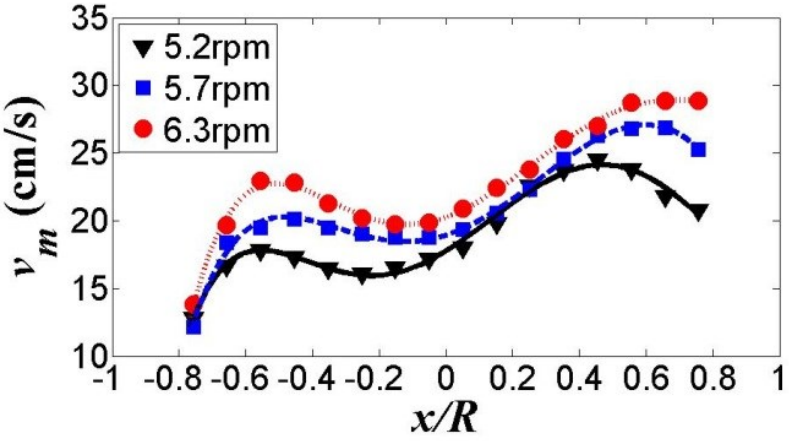

Fig.15 Particle velocity distribution in the radial direction of the drum with 1.25 irregular sands at different rotating velocity from 5.2rpm to 6.3rpm.

IV. PARAMETER DETERMINATION

From Eqs. (5)-(8), it can be seen that the main parameters affecting the spatial filtering characteristics are the size of the spatial filter in the x- and y-directions, X and Y, and the number of slits, n. From a practical point of view, the size of the spatial filter in the y-direction is fixed with the given linear CCD camera. In addition, in the x-direction, we can select X pixels as a spatial filter, and then divide it into 2*n groups; the width of each group is b pixels, the spatial period of the spatial filter p is equal to $2b$ pixels, and $X = n * p$. Therefore, the main parameters affecting the spatial filtering characteristics are the spatial period of the spatial filter, p, and the number of slits, n.

A. Spatial period of spatial filter, p

In order to select appropriate parameters, the irregular particle velocity measurement system depicted in Fig. 5 is employed and the rotating velocities of the drum are fixed. The test lasted for 10 min and a large number of original images were obtained. By setting different parameter n and selecting a different spatial period to the spatial filtering of the original image, each spatial period was tested 10 times; the velocity is calculated by Eq. (1) and shown in Fig. 17. It can be observed that with the increase in spatial period, the measurement velocity increases gradually, and becomes stable when p is larger than 10. Furthermore, if the slit number of the spatial filter n is too small (i.e. $n \leq 4$) the results would be not reliable even with high spatial period. On the other hand, if the spatial period p was too large, the centre frequency of the output signal would be very small. This would lead to a lower resolution and higher error because the fixed frequency resolution of the FFT has a greater effect on the measurement result. Therefore, the optimal thresholds were determined to be between 10 to 36 pixels. Furthermore, it can be seen that for these range of optimal pixels measured velocities overlaps when slit number of the spatial filter are more than 6. Overall that would imply one would need minimally 60-70 pixels per spatial filter, which is only around 8-particle lengths (resolution of imaging is 8 pixel per particle diameter) in the case of our unidirectional SFV method. This is promising results as it similar or slightly better than PIV technique but further studies are needed to elucidate this further.

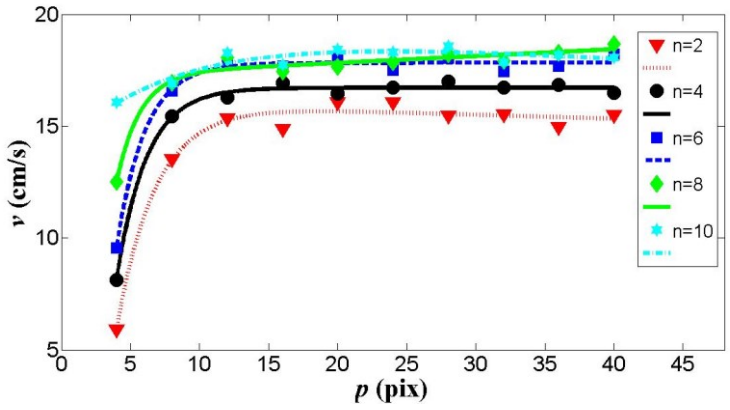

Fig.17 |Measured velocity v vs. spatial period of the spatial filter p with different slit number of the spatial filter n

B. Number of slits, *n*

When the spatial period of spatial filter is fixed, the more slits of the spatial filter, the bigger the filtering window. The size of the filtering window is primarily related to the spatial filtering signal amplitude and main bandwidth. The larger the filtering window, the larger the peak amplitude of the filtering signal; it is helpful to find the peak of the spectrum, and at the same time, the larger the filtering window, the narrower the bandwidth of the signal peak, and the higher the resolution. The measurement point decreases with the number of slits, which leads to a poorer spatial resolution and measurement accuracy.

By setting the spatial period of the spatial filter to p = 32 pixels and changing the number of slits n to the spatial filtering of the original images described in Section 4.1, each slit number was tested 10 times; the centre frequency of the output signal is shown in Fig. 17. With the increase in the number of slits, the measurement results level off at around 4 slits of the spatial filter. The optimal thresholds of the number of slits were determined to be around 8 where the bias of the measurement results from the real value decreases as can be seen in standard deviation of the measurements shown in the figure

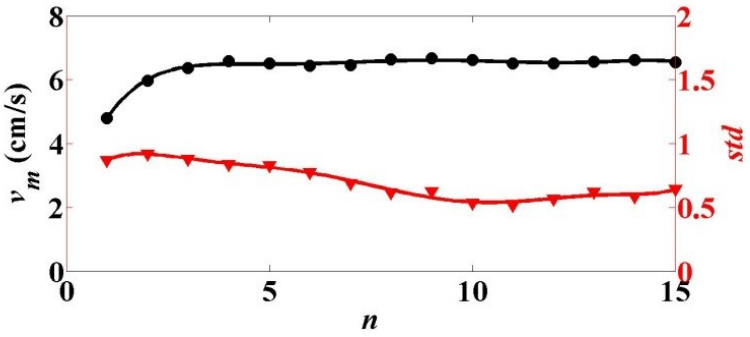

Fig.17 Measured velocity v with associated standard deviation as function of. slit number of the spatial filter n

V. CONCLUSIONS

In this study, the SFV technique has been developed to measure the velocity and its distribution of granular materials (*i.e.* glass beads and sand) using a linear CCD camera. In addition, the energy barycentre correction algorithm was used to enhance the measurement accuracy. Experiments have been conducted to test the accuracy of the method and applicability to the measurement of granular systems. The measurement shows that the velocity and its distributions agree with the theoretical calculation and previous results. The technique has advantage over PTV that each particle does not need to be individually distinguished so it can be applied to smaller particles. The advantage over the PIV is that it is more optically stable and tolerable to lower signal to noise ration from non-uniform illumination among other factors. Furthermore, we analysed the main parameters affecting the spatial filtering characteristics through theoretical analysis experimental verification, and we determined that the optimal thresholds of the spatial period of the spatial filter were between 10 to 36 pixels, and the optimal thresholds of the number of slits were greater than eight. Overall, the reliable velocity measurements are obtained from 60-80 pixels which is only around 8-10 particle length in our current set-up. The major disadvantage of current setup is that the velocity is only measured in direction parallel to the linear CCD pixels array. This issue will be resolved in future work using the improved SFV by utilizing area array CCD to measure the velocity distribution in the whole field of view.

Nomenclature

b	The width of slits of spatial filter
D	inner diameter of the drum
f	centre frequency of output signal
g	output of a slit of spatial filter S_g
$g(x,y)$	output signal obtained from the CCD image sensor
$G_p(\mu,\nu)$	spatial power spectral density function of $g(x,y)$
$h(x,y)$	light intensity distribution of the moving surface image
$H_p(\mu,\nu)$	power spectral density function of $h(x,y)$
L	Length of the drum
M	magnification of the optical system
n	Number of slits of spatial filter
N	FFT point
p	spatial period of spatial filter
S_w	output of a spatial filter
S_g	output of another spatial filter
S_t	output of the differential spatial filter
t	time
$t(x,y)$	light intensity transmittance function of the spatial filter
$T(\mu,\nu)$	Fourier transform of $t(x,y)$
v	the velocity of the object to be tested
w	output of a slit of spatial filter S_w
x	The coordinates of point in the radial direction
X	Size of spatial filter in the x-direction (pixels)
y	The coordinates of point in the axial direction
Y	Size of spatial filter in the y-direction (pixels)
μ	spatial frequencies in the x -directions
ν	spatial frequencies in the y-directions

Acknowledgements

This work has been supported by the National Natural Science Foundation of China (11572201, 91634202) and the Innovation Program of Shanghai Municipal Education Commission (15ZZ072).

References

[1] P.G. de Gennes, Granular Matter: A Tentative View, More Things in Heaven and Earth, Springer1999, pp. 629-643.

[2] R.C. Chen, L.S. Fan, Particle image velocimetry for characterizing the flow structure in three-dimensional gas-liquid-solid fluidized beds, Chemical Engineering Science, 47 (1992) 3615-3622.

[3] Y.C. Chung, S.S. Hsiau, H.H. Liao, J.Y. Ooi, An improved PTV technique to evaluate the velocity

field of non-spherical particles, Powder Technology, 202 (2010) 151-161.

[4] B. Gopalan, F. Shaffer, A new method for decomposition of high speed particle image velocimetry data, Powder Technology, 220 (2012) 164-171.

[5] L.M. Gibson, B. Gopalan, S.V. Pisupati, L.J. Shadle, Image analysis measurements of particle coefficient of restitution for coal gasification applications, Powder Technology, 247 (2013) 30-43.

[6] T. Hagemeier, M. Börner, A. Bück, E. Tsotsas, A comparative study on optical techniques for the estimation of granular flow velocities, Chemical Engineering Science, 131 (2015) 63-75.

[7] S.S. Shirsath, J.T. Padding, H.J.H. Clercx, J.A.M. Kuipers, Cross-validation of 3D particle tracking velocimetry for the study of granular flows down rotating chutes, Chemical Engineering Science, 134 (2015) 312-323.

[8] S. Stanier, J. Dijkstra, D. Leśniewska, J. Hambleton, D. White, D. Muir Wood, Vermiculate artefacts in image analysis of granular materials, Computers and Geotechnics, 72 (2016) 100-113.

[9] X. Xu, Q. Sun, F. Jin, Y. Chen, Measurements of velocity and pressure of a collapsing granular pile, Powder Technology, 303 (2016) 147-155.

[10] D. Gollin, W. Brevis, E.T. Bowman, P. Shepley, Performance of PIV and PTV for granular flow measurements, Granular Matter, 19 (2017) 42.

[11] C. Zhibo, L. Kaigang, O. Mehdi, I. Magued, Guidelines for DIC in geotechnical engineering research, International Journal of Physical Modelling in Geotechnics, 17 (2017) 3-22.

[12] A.V. Orpe, D.V. Khakhar, Scaling relations for granular flow in quasi-two-dimensional rotating cylinders, Physical review E, 64 (2001) 031302.

[13] A.V. Orpe, D.V. Khakhar, Rheology of surface granular flows, Journal of Fluid Mechanics, 571 (2007) 1-32.

[14] H. Capart, D.L. Young, Y. Zech, Voronoï imaging methods for the measurement of granular flows, Experiments in Fluids, 32 (2002) 121-135.

[15] R. Li, H. Yang, G. Zheng, B.F. Zhang, M.L. Fei, Q.C. Sun, Double speckle-visibility spectroscopy for the dynamics of a passive layer in a rotating drum, Powder Technology, 295 (2016) 167-174.

[16] H. Yang, B.F. Zhang, R. Li, G. Zheng, V. Zivkovic, Particle dynamics in avalanche flow of irregular sand particles in the slumping regime of a rotating drum, Powder Technology, 311 (2017) 439-448.

[17] J.T. Ator, Image-Velocity Sensing with Parallel-Slit Reticles, J. Opt. Soc. Am., 53 (1963) 1416-1422.

[18] Y. Aizu, T. Asakura, Principles and development of spatial filtering velocimetry, Applied Physics B, 43 (1987) 209-224.

[19] M.S. Uddin, H. Inaba, Y. Itakura, Y. Yoshida, M. Kasahara, Adaptive computer-based spatial-filtering method for more accurate estimation of the surface velocity of debris flow, Applied optics, 38 (1999) 6714-6721.

[20] X. He, X. Nie, J. Zhou, X. Long, Application of differential weighting function to spatial filtering velocimetry, Optik - International Journal for Light and Electron Optics, 126 (2015) 5678-5681.

[21] Y. Itakura, A. Sugimura, S. Tsutsumi, Amplitude-modulated reticle constructed by a liquid crystal cell array, Applied optics, 20 (1981) 2819-2826.

[22] S. Bergeler, H. Krambeer, Novel optical spatial filtering methods based on two-dimensional photodetector arrays, Measurement Science and Technology, 15 (2004) 1309.

[23] Y. Aizu, T. Asakura, Spatial filtering velocimetry: Fundamentals and applications, Springer series in optical science, vol 116, Springer 2006.

[24] D. Petrak, H. Rauh, Micro-flow metering and viscosity measurement of low viscosity Newtonian fluids using a fibreoptical spatial filter technique, Flow Measurement and Instrumentation, 20 (2009) 49-56.

[25] W. Wang, J. Lin, W. Zhong, L. He, C. Xu, H. Ding, Spatial filtering method for nanofluid velocity measurement based on the area CCD, Chinese Journal of Scientific Instrumentents, 36 (2015) 2495-2501.

[26] C. Xu, J. Li, S. Wang, A spatial filtering velocimeter for solid particle velocity measurement based on linear electrostatic sensor array, Flow Measurement and Instrumentation, 26 (2012) 68-78.

[27] L.N. Zheng, T. Zhang, H.P. Kuang, Image motion velocity measurement technique based on spatial filtering effect of line CCD for aerial camera, Acta Optica Sinica, 32 (2012) 109-115.

[28] S. Hosokawa, T. Matsumoto, A. Tomiyama, Measurement of bubble velocity using spatial filter velocimetry, Experiments in fluids, 54 (2013) 1538.

[29] J. Li, C. Xu, S. Wang, Spatial filtering characteristics of electrostatic sensor matrix for local velocity measurement of pneumatically conveyed particles, Measurement, 53 (2014) 194-205.

[30] C. Xu, B. Zhou, D. Yang, G. Tang, S. Wang, Velocity measurement of pneumatically conveyed solid particles using an electrostatic sensor, Measurement science and technology, 19 (2008) 024005.

[31] X. He, X. Long, X. Nie, J. Zhou, Spatial filtering velocimeter using frequency shifting by the method of rotating kernel, Measurement, 73 (2015) 15-23.

[32] T. Grandke, Interpolation algorithms for discrete Fourier transforms of weighted signals, IEEE transactions on instrumentation and measurement, 32 (1983) 350-355.

[33] C. Offelli, D. Petri, A frequency-domain procedure for accurate real-time signal parameter measurement, IEEE Transactions on Instrumentation and Measurement, 39 (1990) 363-368.

[34] H. Dishan, Phase error in fast Fourier transform analysis, Mechanical Systems and Signal Processing, 9 (1995) 113-118.

[35] G.T. Heydt, P.S. Fjeld, C.C. Liu, D. Pierce, L. Tu, G. Hensley, Applications of the windowed FFT to electric power quality assessment, IEEE Transactions on Power Delivery, 14 (1999) 1411-1416.

[36] X. Zhu, K. Ding, The synthetical comparison of correcting methods on discrete spectrum, Signal Process., 17 (2001) 91-97.

[37] D. Kang, L. Jiang-kai, X. Ming, Time-shifting correcting method of phase difference on discrete spectrum, Applied mathematics and mechanics, 23 (2002) 819-827.

[38] J. Zhou, X. Long, Signal processing of laser Doppler self-velocimeter, Optics & Laser Technology, 42 (2010) 1038-1043.

[39] N. Jain, J.M. Ottino, R.M. Lueptow, An experimental study of the flowing granular layer in a rotating tumbler, Physics of Fluids, 14 (2002) 572-582.

[40] Y.L. Ding, J.P.K. Seville, R. Forster, D.J. Parker, Solids motion in rolling mode rotating drums operated at low to medium rotational speeds, Chemical Engineering Science, 56 (2001) 1769-1780.

[41] O. Dubé, E. Alizadeh, J. Chaouki, F. Bertrand, Dynamics of non-spherical particles in a rotating drum, Chemical Engineering Science, 101 (2013) 486-502.